ACTA METALLURGICA SLOVACA
2022, VOL. 28, NO. 3, 147-150

RESEARCH PAPER

NbC TRANSFORMATION DURING AGING IN HP40-Nb HEAT RESISTANT ALLOY

Matías Humberto Sosa Lissarrague[1], César Armando Lanz[1]

[1] Laboratorio de Metalurgia y Tecnología Mecánica, Departamento de Ingeniería, Universidad Nacional del Sur, Av. L. N. Alem 1253, Bahía Blanca, B8000CPB, Argentina.

*Corresponding author: matias.sosa@uns.edu.ar, tel.: +54 291 4595179, Laboratorio de Metalurgia y Tecnología Mecánica, Departamento de ingeniería, Universidad Nacional del Sur, 8000, Bahía Blanca, Argentina

Received: 15.07.2022
Accepted: 22.08.2022

ABSTRACT

In this work, the evolution of MC-type Nb-rich primary carbides in a 35Ni-25Cr-Nb-type refractory alloy, commonly known as HP40-Nb, and its transformation into Ni-Nb silicide known as G-phase ($Ni_{16}Nb_6Si_7$), has been studied. For this purpose, the experimental technique of scanning electron microscopy was used together with X-ray microanalysis to detect changes in the chemical composition of niobium carbide over time and at a given aging temperature. The microstructure of the studied alloy, in its as-cast condition, consists of an austenitic matrix strengthened by a network of primary eutectic-like carbides rich in chromium and niobium of the $M_{23}C_6$ and MC types, respectively. During aging of the alloy at high temperatures, microstructural changes take place such as the secondary precipitation of $M_{23}C_6$ type carbides and the transformation of the primary Nb-rich carbide towards the Ni-Nb-rich silicide. It has been found that the transformation begins at the interface of the niobium carbides with the matrix, progressing towards their interior with the development of aging.

Keywords: heat resistant alloys; HP40-Nb; G-phase; NbC

INTRODUCTION

For several decades, for reforming hydrocarbons derived from ethylene pyrolysis, reforming furnaces are used. They contain in their heat exchange surfaces, which are necessary for the process, an arrangement of metal tubes that are generally vertical and make up, together with other parts, the surfaces where the reforming reactions take place. The reformer furnace tubes are the most critical components, as they are exposed to severe conditions in terms of high temperature and internal pressure for long time during service, and have inner diameter of 60–200 mm, wall thickness in the range 10–25 mm and length of 10–15 m and with a designed nominal life of up to 100,000 h [1–5]. Since service conditions involve high temperatures and moderate pressures, the materials used for reformer tube demand for higher creep and oxidation resistance. Therefore, the centrifugal cast HP40-Nb alloy, namely 25Cr35Ni1Nb, has been developed by adding a small amount of Niobium into HP40 alloy [5–10]. This austenitic alloy contains in its composition large concentrations of chromium (up to 35%) and nickel (up to 45%), which improves a high resistance to oxidation and carburization [11–13]. One of the main failures that appears in reformer tubes, is caused by the creep phenomenon, which is known to be a combined effect of a high level of temperature (in the order of 60% of melting point) and pressure which causes mechanical stresses that promote permanent deformations in the radial direction of the tube. The morphology of the creep permanent deformation has a direct relationship with the temperature distribution along the wall thickness of the tubes. The combining effects of the high service temperature, mechanical loads due to the internal pressure and the time service, result in catastrophic failures. This may occur due to the accumulation of creep that can generate very serious defects, such as total perforation of the tube wall, excessive ovalization, significant elongation that causes interference with other parts of the furnace, etc. To improve the mechanical resistance of these materials, it has been decided to increase the carbon concentration to 0.4-0.6%. Said modification promotes the strengthening of the alloy by the precipitation technique on the edges or inside the grains of the alloy, of the Cr-rich carbides of the $M_{23}C_6$ and M_7C_3 type [11]. The addition of alloying elements such as Nb, Ti, etc., improves mechanical properties during service through the precipitation of primary carbides of the MC type [14,15].

In the as-cast condition, the microstructure of HP40-Nb alloys consists of an austenitic matrix with intergranular and interdendritic eutectic-like primary Cr-rich carbides of the $M_{23}C_6$ type and Nb-rich carbides of the MC type [6]. During aging, intragranular secondary $M_{23}C_6$ carbides precipitate within the matrix [16,17]. At operating temperatures, in Ni-Cr-Fe based alloys MC-type carbides are thermally unstable, since they would transform into a Ni-Nb silicide, known as G-phase [18–20]. G-phase is known as a Ni-Nb-rich silicide that mainly forms at grain boundaries. The general chemistry of G-phase is proposed as $Ni_{16}Nb_6Si_7$ [3]. For HP40-Nb alloy, this transformation is reported to take place between 700 and 1000°C [4]. There is scarce information about this silicide, which is formed at the interface between the matrix and NbC and continues inward. This transformation causes an increase in the volume of the unit cell and in the interfacial energy, creating compression stresses on the matrix and tensile stresses on the particles, promoting the nucleation of microcracks, which reduce the creep properties of the alloy [3,21,22]. In addition, the formation of the G-phase causes a consumption of Ni and Si from the matrix reducing solid solution hardening [1,11,23,24].

However, it is known that Ti stabilizes NbC carbide and prevents its transformation into G-phase [20,25,26]. The aim of this study is to characterize the evolution of NbC to G-phase transformation during aging at 850ºC at different times by scanning electron microscopy (SEM), and electron probe microanalysis with energy-dispersive X-ray spectroscopy (EDS).

MATERIAL AND METHODS

Specimens of as-cast 35Ni-25Cr-Nb alloy were obtained from a ring extracted from a tube of 110 mm diameter and 11 mm wall thickness and then cut transversely to achieve 12 mm width samples. The chemical composition of the studied material was measured by a SPECTROMAX spectrometer and is indicated in **Table 1**.

Table 1 Chemical composition of HP40-Nb heat resistant alloy (%wt.).

C	Si	Mn	Cr	Ni	Nb	W	Ti	Fe
0.57	2.73	0.76	23.74	37.6	1.26	0.19	0.08	Balance

Aging treatments were made using resistive furnaces in air atmosphere at 850ºC for 48 and 96 h, and then each aged sample was cooled in air. It is important to note that the aged samples do not take into account the effect of mechanical loads or the fluids that circulate inside the tubes. Samples were ground with silicon carbide papers from 240 to 2000 grit. Polishing was done with 1 µm alumina paste. Polished specimens were electrolytically etched with a 10% KOH aqueous solution at 2 V for 14 s. SEM-EDS microanalysis measures were made by a CARL ZEISS electronic microscope, model Sigma, with energy dispersive spectroscope of OXFORD INSTRUMENTS. Samples in the as-cast condition and aged for 48 and 96 h at 850°C were analysed, measuring chemical composition in five several sites into the matrix and the silicide particles in the case of aged samples. Also, linescan of X-ray was done along Nb-rich particles.

RESULTS AND DISCUSSION

As-cast condition

Several SEM-EDS measures were made in an as-cast condition sample in different localizations into the matrix and MC-type primary carbides, in which M corresponds to Nb and Ti atoms. **Fig. 1**, shows a SEM micrograph in back-scattered electron (BSE) mode of the alloy in the as-cast condition.

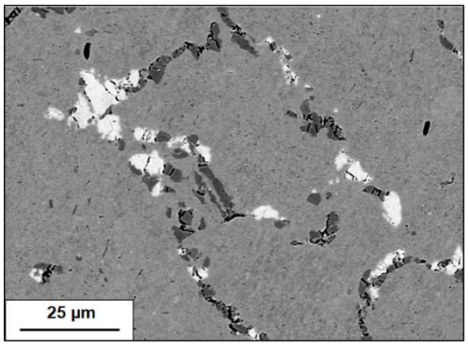

Fig. 1 As-cast SEM (BSE) micrograph of HP40-Nb alloy (1000X).

The mean concentration for each chemical element measured into the matrix for the as-cast condition is presented in **Table 2**.

Table 2 EDS measurements into the matrix of an as-cast sample (%at.).

	Fe	Ni	Cr	Nb	Si
Spectrum 1	38.6	34.1	27.3	0.0	0.0
Spectrum 2	35.3	32.0	22.2	3.5	7.0
Spectrum 3	39.3	33.9	24.8	0.0	2.0
Spectrum 4	40.6	32.0	23.9	0.0	3.4
Spectrum 5	40.6	34.1	25.3	0.0	0.0
Mean	38.9	33.2	24.7	0.7	2.5
Standard deviation	2.2	1.1	1.9	1.6	2.9

The mean concentration for each chemical element measured into MC-type carbides for the as-cast condition is presented in **Table 3**.

Table 3 EDS measurements in MC-type primary carbides on an as-cast sample (%at.).

	C	Ti	Fe	Ni	Nb	Si
Spectrum 1	44.7	16.4	0.9	1.6	34.1	2.3
Spectrum 2	45.8	16.1	0.7	1.7	35.7	0.0
Spectrum 3	42.9	14.2	1.2	1.4	39.4	0.9
Spectrum 4	44.1	15.3	0.8	1.2	37.5	1.1
Spectrum 5	41.3	13.9	1.1	1.3	42.3	0.1
Mean	43.8	15.2	0.9	1.4	37.8	0.9
Standard deviation	1.7	1.1	0.2	0.2	3.2	0.9

As it can be seen, chemical composition corresponds to MC-type carbides, being Ti and Nb equivalent in terms of stoichiometry, adding their individual compositions. However, Fe, Si and Ni were detected probably due to measurements were made near the edges of the particles.

Aging at 850°C for 48 h

On the other hand, by aging heat treatments at high temperatures, the Nb-rich carbides should modify their chemical composition over time, as well as start with the secondary precipitation in the matrix of $M_{23}C_6$ Cr-rich carbides. A SEM (BSE) micrograph of a sample aged 48 h at 850°C can be seen in **Fig. 2**.

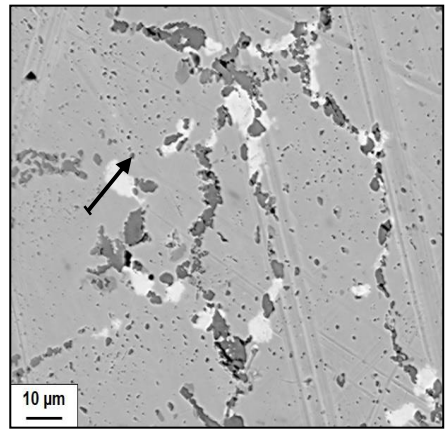

Fig. 2 Microstructure of a sample aged at 850°C for 48 h obtained in the backscattered electron mode, indicating the linear measurement (2500X).

In order to detect the NbC transformation, EDS measurements of chemical composition into Nb-rich phases were made for an aged sample for 48 h at 850°C. For this, their chemical composition was determined in a specific way and along a certain line, as indicated in **Fig. 2**, to know the concentration profile of each element of this phase. These results can be seen in **Table 4** and **Fig. 3**. It is important to highlight that, similarly to what was found for the as-cast condition, for these aging times at 850°C, a high concentration of silicon and nickel is observed at the edges of the Nb-rich particles.

Table 4 EDS measurements in Nb-rich particles for a sample aged 48 h at 850°C (%at.).

	Si	Ni	Nb	C
Spectrum 1	20.0	47.4	15.3	17.3
Spectrum 2	16.8	45.3	14.7	23.2
Spectrum 3	16.3	51.4	21.2	11.1
Spectrum 4	19.3	47.7	19.3	13.7
Spectrum 5	24.7	46.0	13.4	16.0
Mean	19.4	47.5	16.8	16.3
Standard deviation	3.3	2.4	3.3	4.5

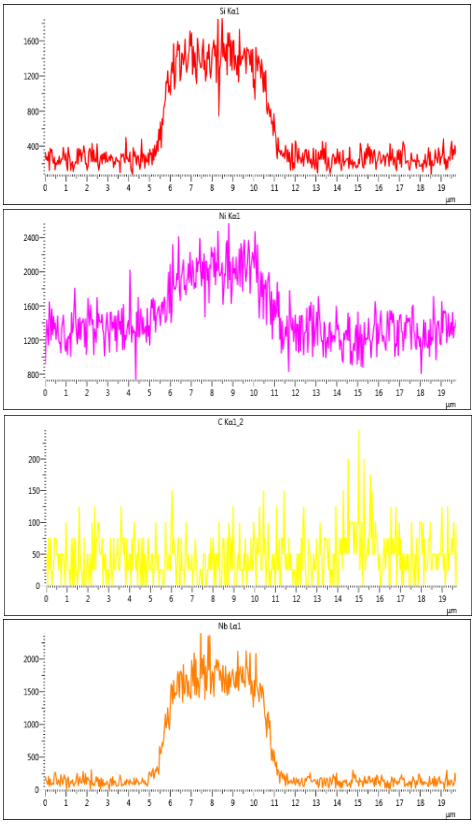

Fig. 3 Linear spectra measured by EDS on a Nb-rich particle for a sample aged at 850°C for 48 h.

Aging at 850°C for 96 h

Similarly, an identical analysis was performed for a sample aged at 850°C for 96 h, in order to detect possible changes in the chemical composition of the phases studied. In this sense, the microstructure of a sample under the mentioned conditions can be seen in **Fig. 4**. In addition, chemical composition was measured along a line by X-ray microanalysis (see **Fig. 5**). At the same time, point spectra were also obtained in Nb-rich particles. In **Table 5**, the results of the analysis for the sample with 96 h of aging at 850°C and the comparison with the G-phase composition can be observed.

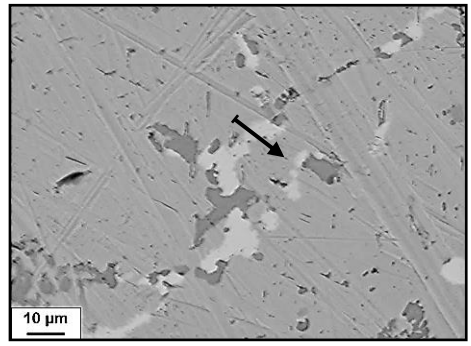

Fig. 4 Microstructure of a sample aged at 850°C for 96 h obtained in the backscattered electron mode, indicating the linear measurement (2500X).

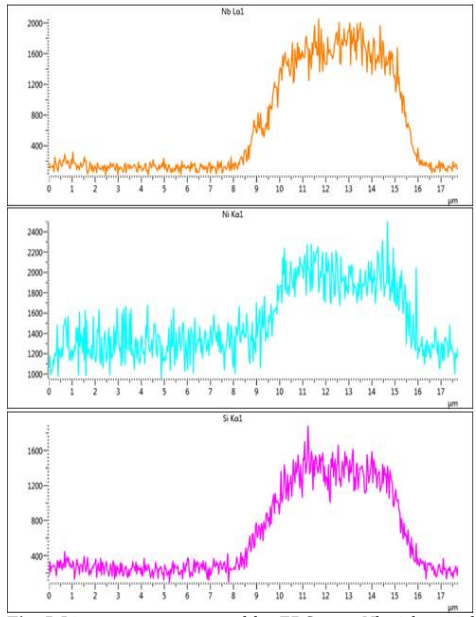

Fig. 5 Linear spectra measured by EDS on a Nb-rich particle for a sample aged at 850°C for 96 h.

As it can be seen, the change in the chemical composition and, therefore, the transformation of the Nb-rich carbide towards G-phase ($Ni_{16}Nb_6Si_7$), is notorious since the mean concentration value of each element is very close to that corresponding to G-phase [3]. In addition, no carbon was found in any of the determinations made on the sample for the aging condition already described.

Table 5 EDS measurements in Nb-rich particles for a sample aged 96 h at 850°C (%at.).

	Si	Ni	Nb
Spectrum 1	23.6	55.8	20.6
Spectrum 2	27.9	52.5	19.6
Spectrum 3	23.3	56.1	20.6
Spectrum 4	25.8	53.6	20.6
Spectrum 5	23.1	56.4	20.5
Mean	24.7	54.9	20.4
Standard deviation	2.0	1.7	0.4
G-phase composition	24.1	55.2	20.7

CONCLUSIONS

From the study of the transformation of the Nb-rich primary carbides in the 35Ni-25Cr-Nb alloy, the following conclusions are reached. As time increases, it can be seen how the transformation of the primary niobium carbide progresses towards a Ni-Nb-rich silicide. This transformation ejects C into the matrix which promotes the nucleation of secondary Cr-rich carbides in the vicinity of the silicide, given the large number of carbon atoms without being combined with other atoms. In turn, the transformation consumes Si and Ni, which are in solid solution in the matrix. The concentration of Nb, Si and Ni, after aging, is maximum in the central part of the particles, while it decreases notably when approaching the interface of said particle with the matrix.

Acknowledgments: Authors are grateful for the support of experimental works by project PGI–SGCyT–UNS 24/J087. C. A. Lanz and M. H. Sosa Lissarrague are researchers in Departamento de Ingeniería in Universidad Nacional del Sur (UNS).

REFERENCES

1. S. Xiang, X. Chen, Z. Fan, T. Chen, X. Lian: Journal of Materials Research and Technology, 18, 2022, 268–281. https://doi.org/10.1016/j.jmrt.2022.02.099.
2. C. Fuyang, J. Chen, B. Shao, Y. Zhou, J. Gong, X. Guo, et al: International Journal of Pressure Vessels and Piping, 192, 2021, 104391. https://doi.org/10.1016/j.ijpvp.2021.104391.
3. M. Abbasi, I. Park, Y. Ro, Y. Ji, R. Ayer, J. H. Shim: Materials Characterization, 148, 2019, 297–306. https://doi.org/10.1016/j.matchar.2019.01.003.
4. C. Fuyang, R. Zhu, P. Zhang, X. Guo, H. Li, L. Geng, et al: International Journal of Pressure Vessels and Piping, 179, 2020. https://doi.org/10.1016/j.ijpvp.2019.104032.
5. H. J. Kim, J. Park, Y. S. Ji, B. M. Jeong, J. Nam, M. G. Jo, et al: Materials Characterization, 176, 2021. https://doi.org/10.1016/j.matchar.2021.111110.
6. M. H. Sosa Lissarrague, S. Limandri, F. Prado, A. C. Picasso: Metallography, Microstructure, and Analysis, 7(3), 2018, 356–362. https://doi.org/10.1007/s13632-018-0448-z.
7. A. C. Picasso, C. A. Lanz, M. H. Sosa Lissarrague, A. D. Garófoli: Journal of Minerals and Materials Characterization and Engineering, 4(1), 2016, 48–61. https://doi.org/10.4236/jmmce.2016.41006.
8. T. Dessolier, T. McAuliffe, W. J. Hamer, C. G. M. Hermse, T. Britton: Materials Characterization, 177, 2021, 111070. https://doi.org/10.1016/j.matchar.2021.111070.
9. J. Guo, T. Cao, C. Cheng, X. Meng, J. Zhao: Microscopy and Microanalysis, 24(5), 2018, 478–487. https://doi.org/10.1017/S1431927618015180.
10. V. H. Dao, J. S. Song, J. Y. Kim, K. B. Yoon: Journal of Mechanical Science and Technology, 33(10), 2019, 4813–4821. https://doi.org/10.1007/s12206-019-0922-9.
11. N. Vaché, P. Steyer, C. Duret-Thual, M. Perez, T. Douillard, E. Rauch, et al: Materialia, 9, 2020. https://doi.org/10.1016/j.mtla.2020.100593.
12. R. Song, S. Wu: Engineering Failure Analysis, 88, 2018, 63-72. https://doi.org/10.1016/j.engfailanal.2018.01.002.
13. S. Y. Kondrat'ev, G. P. Anastasiadi, A. V. Ptashnik, S. N. Petrov: Materialia, 7, 2019. https://doi.org/10.1016/j.mtla.2019.100427
14. M. Wang, D. Flahaut, Z. Zhang, I. P. Jones, Y. L. Chiu: Journal of Alloys and Compounds, 781, 2019, 751–60. https://doi.org/10.1016/j.jallcom.2018.12.095
15. I. A. Sustaita-Torres, S. Haro-Rodríguez, R. Colás: High Temperature Materials and Processes, 37(2), 2018, 133–139. https://doi.org/10.1515/htmp-2016-0112.
16. M. Mohammadnezhad, V. Javaheri, M. Shamanian, S. Rizaneh, J. A. Szpunar: Acta Metallurgica Slovaca, 24(4), 2018, 296–305. https://doi.org/10.12776/ams.v24i4.1160.
17. A. C. McLeod, C. M. Bishop, K. J. Stevens, M. V. Kral: Metallography, Microstructure, and Analysis, 5(3), 2016, 178–187. https://doi.org/10.1007/s13632-016-0274-0.
18. M. P. Arenas, C. J. Pacheco, A. B. Fonseca, F. S. Queiroz, M. Gaudencio, C. B. Eckstein, et al: Journal of Magnetism and Magnetic Materials, 491, 2019, 165578. https://doi.org/10.1016/j.jmmm.2019.165578.
19. P. Jian-hua, C. Zeng, F. Zhi-cao, W. Yu-cheng: International Journal of Pressure Vessels and Piping, 162, 2018, 1–10. https://doi.org/10.1016/j.ijpvp.2018.02.009.
20. G. N. Haidemenopoulos, A. D. Zervaki, H. Kamoutsi, K. Polychronopoulou: European Journal of Materials, 1(1), 2021, 1-22. https://doi.org/10.1080/26889277.2021.1994841.
21. X. Guo, X. Jia, J. Gong, L. Geng, J. Tang, Y Jiang, et al. Materials Science and Engineering A, 690, 2017, 62–70. https://doi.org/10.1016/j.msea.2017.02.057.
22. N. C. de Siqueira, M. P. Arenas, P. D. de Almeida, L. S. Araújo, C. B. Eckstein, L. Nogueira, et al: Journal of Materials Research and Technology, 7(3), 2018, 361–365. https://doi.org/10.1016/j.jmrt.2018.05.014.
23. A. R. Andrade, C. Bolfarini, L. A. M. Ferreira, A. A. A. Vilar, C. D. Souza Filho, L. H. C. Bonazzi: Materials Science and Engineering A, 628, 2015, 176–180. http://dx.doi.org/10.1016/j.msea.2015.01.049.
24. F. Tancret, J. Laigo, F. Christien, R. le Gall, J. Furtado: Materials Science and Technology, 34(11), 2018, 1333–1343. https://doi.org/10.1080/02670836.2018.1449177.
25. S. K Arinova, S. S. Kvon, V. Y. Kulikov, M. M. Abdildina, A. E. Omarova: Metalurgija, 61(2), 2022, 341-343.
26. J. Guo, X. Zhang, C. Li, W. Liu, Z. Zhang: Materials Today Communications, 28, 2021, 102600. https://doi.org/10.1016/j.mtcomm.2021.102600.